J Mater Sci (2009) 44:6302–6309
DOI 10.1007/s10853-009-3868-y

Prediction of hardness minimum locations during natural aging in an aluminum alloy 6061-T6 friction stir weld

W. Woo · H. Choo · P. J. Withers · Z. Feng

Received: 6 July 2009 / Accepted: 3 September 2009 / Published online: 11 September 2009

Abstract This study describes a method that can predict the hardness minimum location as a function of natural aging time in a heat-treatable 6061-T6 Al alloy plate subjected to friction stir welding (FSW). First, temperature distributions were simulated in the FSW plate by finite element modeling. Second, to determine the natural aging kinetics, hardness changes were measured as a function of natural aging time from a number of Al specimens that had been isothermally heat treated at different peak temperatures. Finally, the simulated temperature profiles and the natural aging kinetics were correlated to predict the hardness profiles in the FSW plate. The predicted hardness minimum locations are consistent with the measured hardness profiles in that the hardness moves away from the weld centerline as the aging time increases. Moreover, the predicted hardness minimum is located at the similar position of failure in cross-weld tensile samples.

W. Woo (✉)
Neutron Science Division, Korea Atomic Energy Research Institute, 1045 Daedeok-daero, Yuseong-gu, Daejeon 305-353, South Korea
e-mail: chuckwoo@kaeri.re.kr

H. Choo
Department of Materials Science and Engineering, The University of Tennessee, Knoxville, TN 37996, USA

P. J. Withers
Manchester Materials Science Center, University of Manchester, Grosvenor St., Manchester M1 7HS, UK

Z. Feng
Materials Science and Technology Division, Oak Ridge National Laboratory, Oak Ridge, TN 37831, USA

Introduction

Friction stir welding (FSW) is a solid-state joining process utilizing a rotating tool, which consists of a pin and tool shoulder that apply severe plastic deformation and frictional heating into the base material [1, 2]. The softened material is extruded underneath and around the tool as the tool travels along the welding line and subsequently meets to form a strong metallurgical joint. FSW has been widely used in joining heat-treatable Al alloys for the transportation and aerospace sectors [3, 4]. However, microstructural changes and their resulting effect on mechanical properties are significant in FSW heat-treatable Al alloys. It is mainly due to the growth, dissolution, and re-precipitation of the strengthening precipitates after FSW [5–9]. Thereby, extensive efforts have been made to understand the aging behavior for FSW heat-treatable Al alloys [10–14].

Time-dependent material property change is a critical issue in many end applications. Several process models that describe the aging behavior have been proposed to connect the processing variables with microstructure and hardness/strength of FSW [15–18]. Frigaard et al. developed a process model to estimate the evolution of re-precipitation and resultant hardness distributions in FSW AA6082-T6 and AA7108-T79 alloys [15]. Shercliff et al. suggested a method to predict the microstructural changes in FSW based on the softening behavior of precipitates in 2xxx Al alloys [16]. Robson and Sullivan proposed a natural aging process model considering the strength loss due to the dissolution and coarsening of the precipitates in FSW AA7449 [17]. Using similar approaches, Peel et al. were able to predict the distribution of hardness in dissimilar AA6082-AA5083 FSW prior to, and subsequent to, natural aging [18]. These models describe the dissolution/coarsening and

re-precipitation behavior in FSW based on classical thermodynamics and diffusion [19–21].

However, numerical tracking of the precipitation behavior requires a relatively sophisticated analysis with unclear assumptions. Moreover, those prior process models have limited to predict the hardness profiles *before* and *after* natural aging. It is suspicious how the aging response is *during* natural aging for the FSW heat-treatable Al alloys. Such time-dependent model is necessary and valuable aid on the mechanical evaluation of FSW as a function of natural aging time. Subsequently, one can determine when the material properties have sufficiently stabilized and represent the fully natural aged condition. It is, therefore, of practical value to ask whether a semiempirical method can be developed to provide a predictive capability of the hardness profiles as a function of natural aging time.

In this study, we present the results of: (1) simulated temperature profiles in a FSW 6061-T6 Al alloy plate using finite element (FE) modeling, (2) the natural aging kinetics (a constitutive relationship between the temperature and hardness at a given time) of Al 6061-T6 alloy based on a series of hardness measurements performed as a function of time using isothermal furnace heat-treated Al specimens, and (3) predicted hardness profiles of the FSW plate under the natural aging condition using the correlation between the simulated temperature profiles and the natural aging kinetics. In this regard, we can predict how the hardness minimum location changes with time, which is important to determine the fracture location in the FSW heat-treatable Al plate.

Experimental procedures

Friction stir welding

6061 Al alloy rolled plate was given a T6 (peak aged) heat treatment, namely, solution heat treated and aged for 6 h at 185 °C. The nominal chemical composition in weight percent is 1.0 Mg, 0.6 Si, 0.3 Cu, and balance Al. The Al plate typically contains precipitates (GP-I, β'', β', and β-Mg_2Si) [5, 6]. The grains in the parent plate were elongated along the rolling direction being about 200 μm in diameter. The FSW was performed along the centerline of a single ($306 \times 306 \times 6.5$ mm^3) plate (Fig. 1a) using the following parameters: 4.7 mm/s traveling speed, 1,250 rpm clockwise rotation speed, and 8,000 N compressive force using a tool with 19.05 mm shoulder diameter and 6.35 mm pin diameter of 6.23 mm length. Note that the tool was made of an H-13 tool steel and the traveling direction of the tool was parallel to the rolling direction of the parent plate. The temperature distributions were measured during FSW using

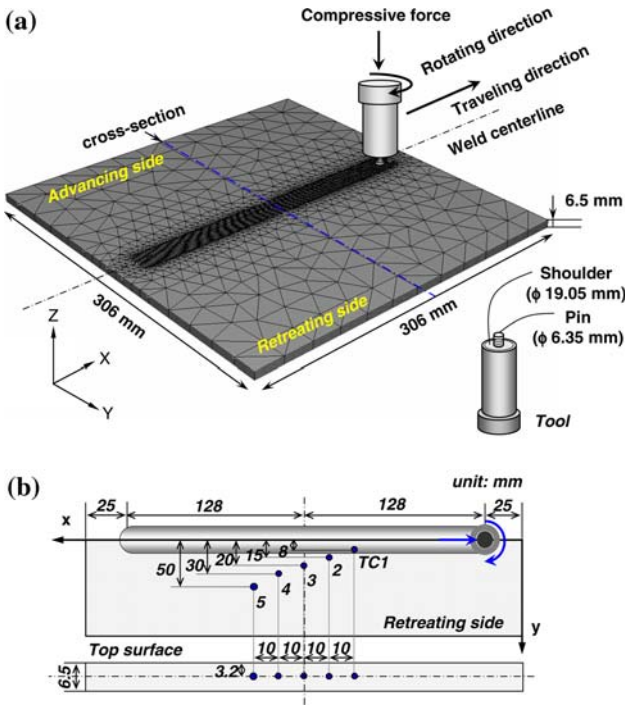

Fig. 1 **a** Schematic of the FSW and tool geometry. The FSW 6061-T6 Al alloy plate was meshed for the FE modeling. **b** Placement of thermocouples. Thermocouples (marked TC1–5) were inserted 3.2 mm below the top surface of the Al plate

eight thermocouples (TC1–8), five positioned at 8, 15, 20, 30, and 50 mm from the weld centerline on the retreating side of the plate (Fig. 1b) and three more thermocouples were positioned at 15, 20, and 30 mm on the advancing side. Note that the retreating side is denoted as the positive *y*-direction (advancing side is negative) throughout the article. Each TC was inserted 3.2 mm below the top surface of the plate.

After FSW, the sample was cut across the mid-length of the weld for microstructural characterization. Vickers microhardness (H_V) was measured along the *y*-direction of the mid-thickness on the polished surface with 0.25 mm horizontal indent spacings using 100 g of applied load. Note that hardness profiles were measured at about 10^4 s (4 h) and 10^7 s (8 months) after FSW. In addition, a total of five lines were measured across the thickness of the plate to construct a hardness map. Two cross-weld tensile specimens were also prepared about 10^7 s after FSW to observe the fracture locations. The tensile specimens were prepared using EDM with the dimension of 12.5 mm wide, 6.5 mm thick, and 50 mm long in the gage section following the ASTM E 8M-04. Tensile tests were performed at room temperature using a Material Test System load frame with hydraulic wedge grips at a constant crosshead velocity providing an initial strain rate of 10^{-3} s^{-1}.

Isothermal furnace heat treatments

The natural aging kinetics of the 6061-T6 Al alloy was investigated using prior isothermal heat-treated specimens. A total of five specimens having the dimension of $20(x) \times 50(y) \times 6.5(z)$ mm^3 were prepared from the as-received Al plate. The surface of each specimen was polished and immersed in a salt bath of the furnace. The peak temperature of the furnace was heated up to 250, 350, 450, 500, and 550 °C with the control of a k-type thermocouple. Note that each specimen experienced the peak temperature isothermally for about 10 s and water quenched in about 20 s of leaving the furnace to simulate the thermal history of FSW. Hardness measurements were performed repeatedly after the cooling until about 10^6 s. It established the natural aging kinetics, which is the relationship between the heat-treatment temperature and hardness as a function of natural aging time in the 6061-T6 Al alloy plate. Note that the presented hardness here is an average of the five times measurements on the polished surface along the mid-thickness of each specimen.

Finite element modeling

A three-dimensional FE model was created using a commercial FE analysis code, ABAQUS 6.7, to determine the thermal evolution caused by FSW [22–30]. Note that the modeling included only the thermal heat input and ignored the metal flow caused by the stirring of the tool. First, the FSW plate was meshed using a 6-node triangular prism element (type DC3D6) and an 8-node hexahedra brick element (type DC3D8) outside and underneath the tool shoulder, respectively (Fig. 1a). The tool was not included in the model. Second, the total heat input (Q) from the FSW tool was continuously put into the nodes of the meshed elements using an ABAQUS subroutine [29]. It is assumed that 90% of Q was imposed on the surface nodes over the tool shoulder and 10% on the volumetric nodes of the tool pin [31]. The heat flow at the nodes was treated as a heat conduction problem. Finally, when the tool moves along the weld centerline, the temperature distributions were calculated for a given welding speed of FSW. The boundary condition of the plate surface was a convection condition. The convective heat coefficient was selected to be 30 W/m^2°C for the top and side surface of the plate, which is typical for the natural convention between Al and air, while 200 W/m^2°C was used for the bottom surface due to the contact with the steel backing plate [22].

A precise determination of Q during FSW is critical because the heat input and simulated temperature will be used as a key factor to predict the hardness. A numerical heat flow model proposed by Frigaard et al. can calculate Q [15]. In brief, Q can be generated by the friction between the plate and the tool bottom surface and calculated based on the torque required to rotate the circular shaft with an axial load following:

$$Q = \frac{4}{3}\pi^2 \mu P N R^3 \quad (1)$$

where μ is the friction coefficient (taken to be 0.4 [27]), P is the constant loading pressure (28.3 MPa), N is the rotational speed (20.8 s^{-1}), and R is the tool shoulder radius (9.5×10^{-3} m). As a result, a first estimate of Q was around 2,200 W under the current conditions. Khandkar et al. determined Q using the torque (M, Nm) of the tool during FSW [26]. Q was given by the measured input torque multiplied by the rational speed (N, 1/s): $Q = 2\pi NM$ [26]. In this experiment, the average torque (M) was recorded as 18.8 Nm during FSW and Q was calculated as 2,100 W. Note that 13% of the heat loss was considered due to heat conducted through the tool during FSW.

To confirm the Q obtained by the above numerical prediction methods, we used an inverse thermal FE modeling approach [22, 23]. The inverse modeling scheme is as follows: (i) four temperature profiles were simulated by FE modeling on the basis of different Q values (Q = 2,200; 2,000; 1,750; and 1,550 W), (ii) the resulting thermal predictions were compared to the measured temperatures profiles, and (iii) finally, an appropriate Q was selected on the basis of the best fit.

Results and discussion

Thermal profiles during friction stir welding

Figure 2a shows the peak temperature distributions during FSW as a function of distance from the weld centerline. The simulated peak temperature is the FE response at the nodes located 3.2 mm below the top surface. It is evident that the best agreement between the measurements and predictions occurs when the Q is taken to be 2,000–2,200 W. At this level of heat input, the peak temperature at the mid-thickness of the FSW plate is predicted to be around 480–520 °C at the centerline ($y = 0$ mm). It is worth noting that the temperature range is reasonable when calculating using the empirical relationship between the peak temperature (T) and rotating (ω)/traveling (v) speed parameters as shown in Eq. 2 of [1]: $T = K(\omega/v \times 10^4)^{\alpha} \cdot T_m$. Following the equation, T was calculated as 490 °C when used $K = 0.75$, $\alpha = 0.04$, and T_m (melting temperature) = 660 °C. Figure 2b shows the comparison of the measured and predicted (Q = 2,200 W) temperature profiles as a function of time at various positions on the retreating side. Unfortunately, the thermocouple located

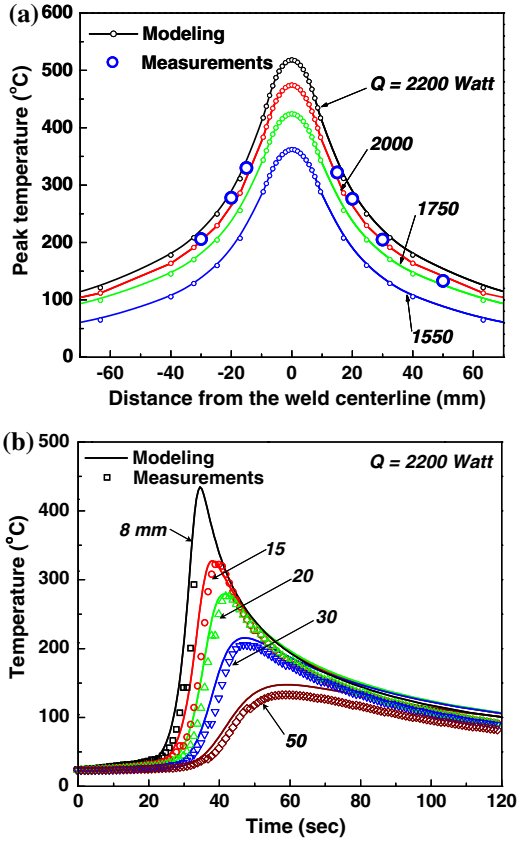

Fig. 2 **a** Simulated peak temperature distributions as a function of distance from the weld centerline in four different cases (Q = 2,200; 2,000; 1,750; and 1,550 W) during FSW. Measured peak temperatures were marked at seven different locations. **b** Measured and simulated temperature variations as a function of time during FSW at 8, 15, 20, 30, and 50 mm from the weld centerline on the retreating side

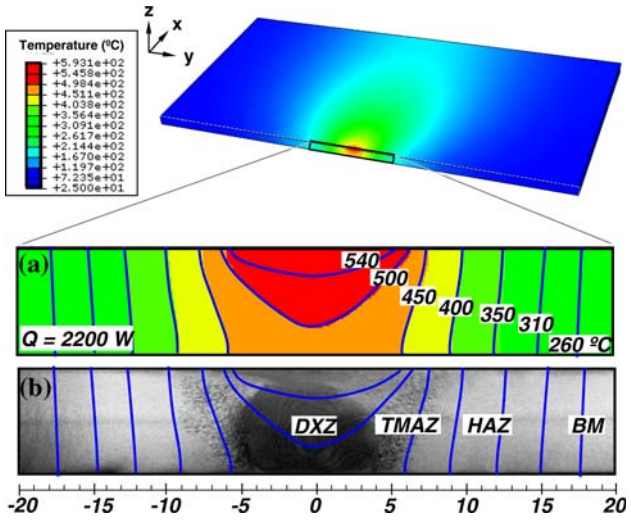

Fig. 3 **a** Simulated temperature distributions in the cross-section of the 6061-T6 Al alloy during FSW using FE modeling. **b** The microstructure of the FSW 6061-T6 Al alloy with the same temperature contour shown in (**a**). The four typical regions are marked on the cross-section: the base material (*BM*), heat-affected zone (*HAZ*), thermomechanically affected zone (*TMAZ*), and dynamic recrystallized zone (*DXZ*)

8 mm from the weld centerline broke as the tool passed over it and so the peak temperature is not available. Overall, the 2,200-W curve shows good agreement with the experimental measurements.

Figure 3a shows the predicted temperature distributions when the tool is coincident with the viewed cross-section of the plate. Unsurprisingly, the highest temperatures are developed near the top surface due to the contact with the tool shoulder and gradually decrease away from the weld centerline. A difference of about 140 °C was simulated through the thickness of the plate at the centerline, i.e., about 590 °C at the top surface and 450 °C at the bottom. In Fig. 3b, the simulated temperature profiles are superimposed on the microstructure linking the peak temperatures to the characteristic regions. It shows that the dynamic recrystallized zone (DXZ) experienced about 480–550 °C, the thermomechanically affected zone (TMAZ) about 430–480 °C, and the heat-affected zone (HAZ) less than 430 °C.

Softening and natural aging kinetics

Figure 4a shows the hardness changes as a function of natural aging time measured from the isothermally heat-treated 6061-T6 Al alloy specimens exposed at different temperatures from 250 to 550 °C. In the case of the 550 °C heat treatment, there is a significant decrease in hardness at room temperature compared to the initial hardness (110 H_V) and increases up to about 75 H_V after 10^6 s of natural aging. In contrast, for the sample exposed to 350 °C, the loss of hardness is less marked and it recovers much more slowly to a lower level ($\sim$70 H_V).

Several studies suggest that significant dissolution and reversion of fine precipitates (β'') will occur with increasing prior exposure temperature [15–18]. This explains the more loss of hardness and recovery of the hardness during natural aging when exposed at the higher temperature as shown in Fig. 4a; whereas, the limited softening and recovery capabilities of the specimens exposed to the low temperatures are due to incomplete dissolution of hardening precipitates and the formation of nonhardening precipitates [6, 12]. Thus, it has been reported that a very complex series of growth, dissolution, and re-precipitation phenomena occur for the whole sequence of precipitates during softening and hardness recovery [15–21].

Rather than simulate this whole natural aging process, the softening and natural aging kinetics of the heat-treatable Al alloys can be empirically modeled using the

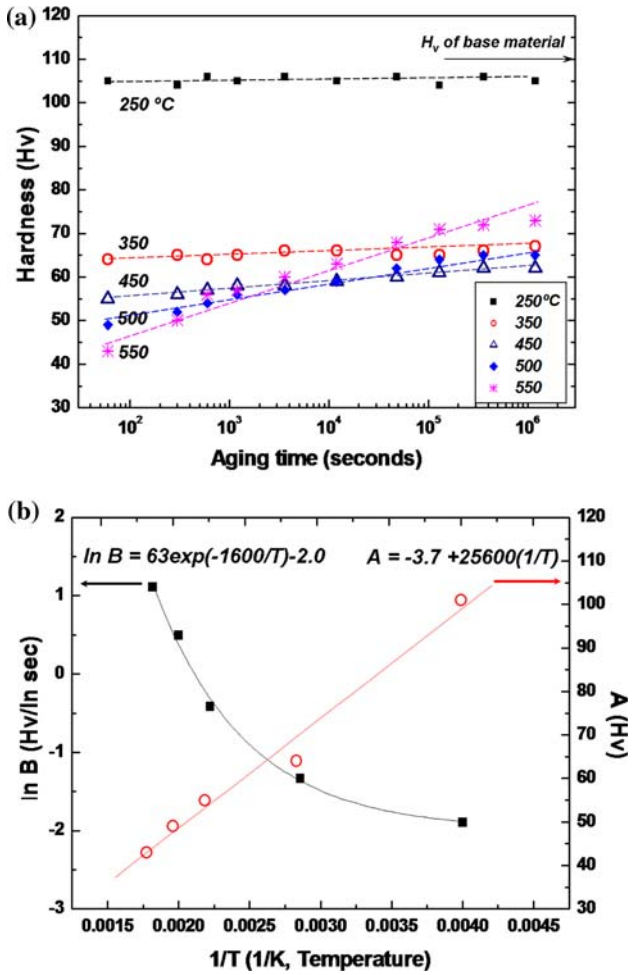

Fig. 4 **a** Hardness variation as a function of natural aging time after heat treatments of 6061-T6 Al alloy samples at various temperatures raging from 250 to 550 °C. **b** Arrhenius plot for the initial hardness (A_T) and aging kinetics (B_T) as a function of inverse temperature (1/T)

relationship between hardness (H_V) and natural aging time (t, s) for a given heat-treatment temperature (T, K) [32, 33]:

$$H_V = A_T + B_T \cdot \ln t \tag{2}$$

where A_T is the initial hardness at 1 s and B_T is the slope coefficient (H_V/ln s) of natural aging. Figure 4b shows the initial hardness constant (A_T) and the aging kinetics (B_T) as a function of heat-treatment temperature. It was obtained from the softening and hardening results as shown in Fig. 4a. Linear and exponential fitting results provide the relationships:

$$A_T = -3.7 + 25600\frac{1}{T}, \quad \ln B_T = 63\exp(-1600/T) - 2.0 \tag{3}$$

Consequently, the constitutive relationship has been achieved correlating the hardness (H_V), heat-treatment temperature (T), and aging time (t) for the Al 6061-T6 alloy in Eq. 2.

Prediction and measurements of the hardness profiles

Hardness variations of the FSW heat-treatable Al alloy strongly depend on the natural aging time and/or heat input [13, 15]. Table 1 summarizes the predicted hardness variations at $t = 1$, 10^4, and 10^7 s using the A_T and B_T. Note that the selected peak temperatures are shown in Fig. 3a, and the hardness was calculated using Eqs. 2 and 3 at different natural aging times. The hardness data at 1 s gives an impression of the hardness immediately after welding even though the FSW may not be cooled instantaneously. The predicted hardness variations were presented on the cross-section of the FSW (Fig. 5a). Note that the hardness variations were marked on the thermal profiles derived from the FE simulation of the 2,200-W heat-input case as

Table 1 Hardness variations as a function of the natural aging time

FSW peak temp. (°C)	A_T (H_V)	B_T (H_V/ln s)	H_V after aging time of:		
			1 s	10^4 s	10^7 s
540	43	3.1	43	69	88
500	48	1.4	48	61	70
450	53	0.7	53	60	66
400	59	0.4	59	63	65
350	68	0.3	68	71	72
310	79	0.2	79	81	82
260	94	0.1	94	96	97

The initial hardness constant (A_T) and the aging kinetics (B_T) were calculated using Eq. 3, and the natural aging hardness (H_V) was obtained from Eq. 2 for a given peak temperature and aging time

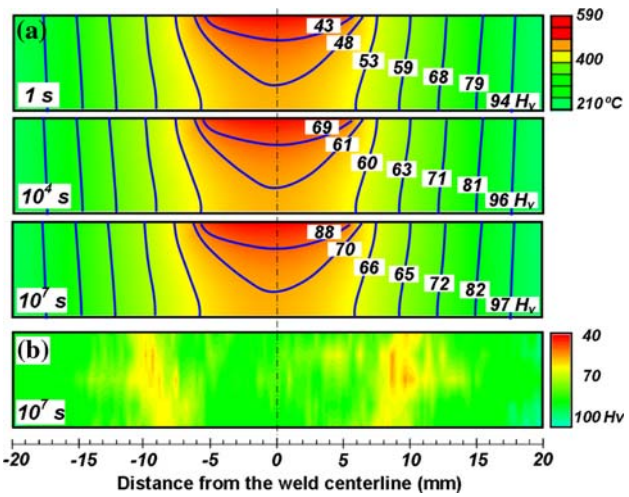

Fig. 5 **a** Predicted hardness variations as a function of natural aging time (nominally 1, 10^4, 10^7 s) in 2,200-W heat-input case. **b** Mapping of the hardness using the measurements across the FSW specimen 10^7 s after FSW

shown in Fig. 3a. The peak temperature experienced gradual increase toward the centerline and the predicted initial hardness falls to 43 H_V near the weld centerline. Upon natural aging it is predicted to recover to 69 H_V at 10^4 s and 88 H_V at 10^7 s, while the hardness beyond 15 mm from the centerline remains essentially unchanged. This trend in hardness evolution causes the minimum hardness location to move with time. To validate the hardness predictions, the hardness map was measured at 10^7 s after FSW (Fig. 5b). Note that the yellow-colored regions indicate where the hardness is below 70 H_V. It shows that the hardness minimum is located at about 9–10 mm from the centerline in good agreement to the simulated one. It is also the case of the two other heat-input cases (Q = 2,000 and 1,750 W) presented in Fig. 6. By comparing the three heat-input cases, it clearly shows that the hardness minimum moves outward; the higher the heat input the longer is the natural aging time.

Since the hardening precipitates primarily govern the strength of heat-treatable Al alloys, the location of the hardness minimum is a potential fracture location during transverse tensile loading in the FSW heat-treatable Al alloys [30, 34]. Figure 7 compares between the hardness predictions and measurements profiled along the mid-thickness of the cross-section in FSW. Note that the predicted hardness within ±4 mm was profiled using the maximum temperature considering significant metal flow within the DXZ. The predicted result shows that the hardness minimum is changed from 8 mm at 10^4 s to 10 mm at 10^7 s after FSW. It is consistent with the hardness measurement results. Moreover, cross-weld tensile tests on samples at 10^7 s showed the fracture locations to be about 10 mm from the weld centerline on the advancing side in accordance with the current predictions.

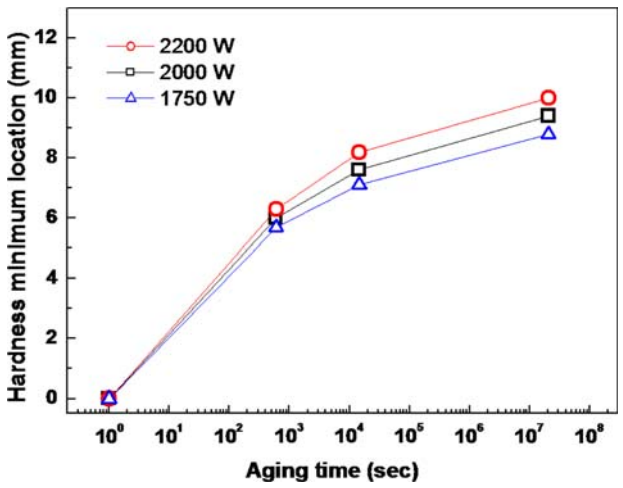

Fig. 6 Predicted hardness minimum locations as a function of natural aging time (1, 10^3, 10^4, and 10^7 s) under three different total heat input cases (Q = 2,200; 2,000; and 1,750 W)

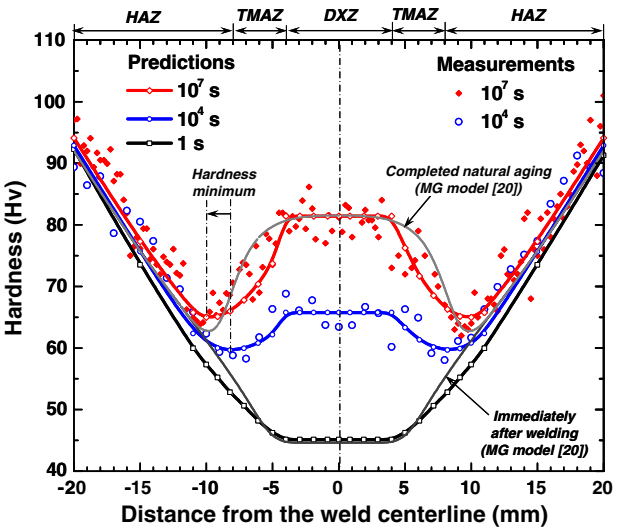

Fig. 7 The measured and predicted hardness profiles at 1, 10^4, and 10^7 s after FSW. These are compared to the hardness profiles predicted by the MG process model in [20]

These changes of the hardness minimum location are related to the different natural aging responses in each characteristic region of FSW. The DXZ is the region softened the most due to the complete dissolution of precipitates at the highest peak temperature (over 480 °C) during FSW. Subsequently, the DXZ has the highest capacity for re-precipitation and increases of the hardness when it fully natural aged [13, 35]. Similarly, the hardness in the TMAZ was increased under natural aging, although it is not as much as that of the DXZ. As a result, the hardness minimum location moves outward the HAZ, which is observed in the current experimental and prediction results (Fig. 7).

Comparison between a prior and the current predictions

For comparison, we simulate the hardness profiles for the current case (Q = 2,200 W) using the Myhr and Grong's (MG) model [20] (Fig. 7). In brief, the MG method theoretically calculates the reaction kinetics of the precipitates in fractions under the softening and hardening conditions, and predicts the hardness profile using the following equation [20]:

$$HV = HV_{min} + (HV_{max} - HV_{min})\alpha \quad (4)$$

where HV_{max} (110 H_V) is the initial hardness of the base metal, and HV_{min} (45 H_V) is the hardness in the absence of the precipitates. Note that the fraction of precipitates (α) under the dissolution or hardening condition was adopted from [20]. Overall, it is a good agreement between the hardness profiles simulated using the MG model and current method (Fig. 7). There is a slight discrepancy between

the two hardness profiles at the same aging time. It could be attributed to the different peak temperature and subsequent hardness aging responses in each location of the current method, whereas the GM model simultaneously switches the hardness profile from the softening to recovery curve at a point where the hardness has the same value [20]. In the end, it should be mentioned that the current method enables us to simulate the hardness profiles and minimum locations *throughout* the natural aging in FSW Al 6061-T6 alloy, while the MG model can simulate the hardness immediately after the welding and after the completion of the natural aging process (Fig. 7).

Conclusions

Hardness variations during natural aging were predicted in a FSW of the heat-treatable 6061-T6 Al alloy using a FE model of the thermal history and the natural aging kinetics obtained by isothermal furnace heat treatments.

1. In situ temperature measurement data during FSW was used to validate the FE modeling. The peak temperature profiles were calculated for each characteristic region in the FSW: DXZ about 480–550 °C, TMAZ about 430–480 °C, and HAZ less than 430 °C for the current conditions.
2. The hardness measurements were performed as a function of natural aging time using a number of isothermally heat-treated Al alloy samples in a furnace at various temperatures. The results provide the initial hardness constant (A_T) due to the softening and logarithmic aging response (B_T) of strengthening precipitates in 6061-T6 Al alloy: $A_T = -3.7 + 25{,}600\ (1/T)$, $\ln B_T = 63\exp(-1600/T) - 2.0$, where T is the heat-treatment temperature (K).
3. The simulated temperature profiles in the FSW plate and the natural aging kinetics were correlated to predict the hardness variations as a function of aging time after FSW. The simulated profiles for the 2,200-W heat-input case show that the hardness minimum location was changed from the TMAZ (8 mm) at 10^4 s to the HAZ (10 mm) at 10^7 s. It is a good agreement with the hardness measurements and fracture locations in the tensile tests of FSW.
4. The current model successfully predicted the complete time-dependent hardness minimum locations at the three different heat-inputs cases (1,750; 2,000; and 2,200 W) in FSW Al 6061-T6 alloy.

Acknowledgements This work was supported by the NSF International Materials Institutes (IMI) Program under contract DMR-0231320. This research was sponsored by the Laboratory Directed Research and Development program of Oak Ridge National Laboratory (ORNL), managed by UT-Battelle, LLC for the U.S. Department of Energy under Contract No. DE-AC05-00OR22725. WW was supported by Nuclear Research and Development Program of the Korea Science and Engineering Foundation funded by the Korean government. PJW is grateful to the EPSRC Lightweight alloys portfolio grant for financial support. The authors would like to thank B. Lovell, S. A. David, C. J. Rawn, and A. Frederick for their help. WW is especially grateful to David Richards for help with the modeling during his visit to Manchester.

References

1. Mishra RS, Ma ZY (2005) Mater Sci Eng R 50:1
2. Threadgill PL, Leonard AJ, Shercliff HR, Withers PJ (2009) Int Mater Rev 54:49
3. Thomas WM, Nicholas ED (1997) Mater Des 18:4
4. Smith IJ, Lord DDR (2008) In: Seventh international symposium on friction stir welding, TWI, Japan
5. Murr LE, Liu G, Mcclure JC (1998) J Mater Sci 33:1243 10.1023/A:1004385928163
6. Sato YS, Kokawa H, Enomoto M, Jogan S (1999) Metall Mater Trans A 30:2429
7. Jata KV, Sankaran KK, Ruschau JJ (2000) Metall Mater Trans A 31:2181
8. Sutton MA, Yang B, Reynolds AP, Taylor R (2002) Mater Sci Eng A 323:160
9. Su JQ, Nelson TW, Mishra R, Mahoney M (2003) Acta Mater 53:713
10. Genevois C, Deschamps A, Denquin A, Doisneau-Cottignies B (2005) Acta Mater 53:2447
11. Kamp N, Sullivan A, Tomasi R, Robson JD (2006) Acta Mater 54:2003
12. Dumont M, Steuwer A, Deschamps A, Peel M, Withers PJ (2006) Acta Mater 54:4793
13. Woo W, Choo H, Brown DW, Feng Z (2007) Metall Mater Trans A 38:69
14. Simar A, Bréchet Y, de Meester B, Denquin A, Pardoen T (2007) Acta Mater 55:6133
15. Frigaard Ø, Grong Ø, Midling OT (2001) Metall Mater Trans A 32:1189
16. Shercliff HR, Russell MJ, Taylor A, Dickerson TL (2005) Méc Ind 6:25
17. Robson JD, Sullivan A (2006) Mater Sci Technol 22:146
18. Peel MJ, Steuwer A, Withers PJ (2006) Metall Mater Trans A 37:2195
19. Shercliff HR, Ashby MF (1990) Acta Metall Mater 38:1789
20. Myhr OR, Grong Ø (1991) Acta Metall Mater 39:2693
21. Bjørneklett BI, Grong Ø, Myhr OR, Kluken AO (1999) Metall Mater Trans A 30:2667
22. Chao YJ, Qi X (1998) J Mater Process Manuf Sci 7:215
23. Chao YJ, Qi X, Tang W (2003) Trans ASME 125:138
24. Ulysse P (2003) Int J Mach Tools Manuf 42:1549
25. Chen CM, Kovacevic R (2003) Int J Mach Tools Manuf 43:1319
26. Khandkar MZH, Khan JA, Reynolds AP (2003) Sci Technol Weld Join 8:165
27. Song M, Kovacevic R (2004) Proc Inst Mech Eng Part B: J Eng Manuf 218:17
28. Nandan R, Roy GG, Debroy T (2006) Metall Mater Trans A 37:1247
29. Richards DG, Prangnell PB, Withers PJ, Williams SW, Wescott A, Oliver EC (2006) Mater Sci Forum 524–525:71
30. Feng Z, Wang XL, David SA, Sklad PS (2007) Sci Technol Weld Join 12:348

31. Schmidt H, Hattel J, Wert J (2004) Model Simul Mater Sci Eng 12:143
32. Esmaeili S, Lloyd DJ, Poole WJ (2003) Acta Mater 51:3467
33. Mrówka-Nowotnik G, Sieniawski J (2005) J Mater Process Technol 162:367
34. Nelson TW, Steel RJ, Arbegast WJ (2003) Sci Technol Weld Join 8:283
35. Linton VM, Ripley MI (2008) Acta Mater 56:4319